

## Residual Carbon in Oxygen-Neon White Dwarfs and its Implications for Accretion-Induced Collapse

JOSIAH SCHWAB<sup>1,\*</sup> AND KYLE AKIRA ROCHA<sup>1,2</sup><sup>1</sup>*Department of Astronomy and Astrophysics, University of California, Santa Cruz, CA 95064, USA*<sup>2</sup>*Department of Physics and Astronomy, Northwestern University, 2145 Sheridan Road, Evanston, IL 60208, USA*

## ABSTRACT

We explore the effects of the residual  $^{12}\text{C}$  present in oxygen-neon white dwarfs (ONe WDs) on their evolution towards accretion-induced collapse (AIC). We produce a set of ONe WD models using *MESA* and illustrate how the amount and location of the residual carbon depends on the initial mass of the star and assumptions about rotation and convective overshooting. We find a wide range of possible  $^{12}\text{C}$  mass fractions roughly ranging from 0.1 to 10 per cent. Convection and thermohaline mixing that occurs as the ONe WDs cool leads to nearly homogeneous interior compositions by the time that AIC would occur. We evolve these ONe WD models and some toy WD models towards AIC and find that regardless of the carbon fraction, the occurrence of Urca-process cooling due to  $^{23}\text{Na}$  implies that the models are unlikely to reach carbon ignition before electron captures on  $^{24}\text{Mg}$  occur. Difficulties associated with modeling electron-capture-driven convective regions in these ONe WDs prevent us from evolving our *MESA* models all the way to thermonuclear oxygen ignition and the onset of collapse. Thus, firm conclusions about the effect of carbon on the final fates of these objects await improved modeling. However, it is clear that the inclusion of residual carbon can shift the evolution from that previously described in the literature and should be included in future models.

*Keywords:* stars: evolution — white dwarfs

## 1. INTRODUCTION

Stellar evolution provides a variety of pathways that produce degenerate cores with oxygen-neon (ONe) compositions and masses near the Chandrasekhar mass. When the central density of the core reaches a critical value  $\sim 10^{10} \text{ g cm}^{-3}$ , electron-capture reactions on isotopes such as  $^{24}\text{Mg}$  and  $^{20}\text{Ne}$  set in motion a chain of events that lead to the destruction of the star (Miyaji et al. 1980; Miyaji & Nomoto 1987). This has generally been thought to involve the collapse of the core and the formation of a neutron star (NS).

Single stars with masses in the range  $\approx 8 - 10 M_{\odot}$  develop degenerate ONe cores while avoiding oxygen ignition (e.g., Nomoto 1984; Garcia-Berro & Iben 1994) and thus have the potential to produce an electron-capture supernova (ECSN; Nomoto 1987; Hashimoto et al. 1993). A related process can occur in binary systems that produce an ONe WD with a close companion, such that material is added to the ONe WD

(Nomoto et al. 1979): this could be a system where a non-degenerate companion donates material onto the WD or in a double WD system that merges. These two binary scenarios, which are in close analogy to the single and double degenerate scenarios for Type Ia supernovae (e.g., Maoz et al. 2014), are referred to as accretion-induced collapse (AIC) and merger-induced collapse (MIC) respectively. AIC and MIC, by virtue of operating in old stellar populations, have long been invoked as a method of producing young NSs in globular clusters (Lyne et al. 1996; Boyles et al. 2011). Stellar population synthesis calculations indicate AIC and MIC may occur at  $\approx 10\%$  of the thermonuclear supernova rate (Ruiter et al. 2018).

The final phase of ECSN/AIC/MIC occurs when the density-driven initiation of exothermic electron-capture reactions causes the thermonuclear ignition of oxygen fusion at or near the center of the ONe core. This leads to the development of an oxygen-burning deflagration wave that then propagates outward through the star. Further electron-capture reactions on the deflagration ashes sap the pressure support. The final fate of the star is set by a competition between these two processes. The timescales over which these processes occur are sensitive

Corresponding author: Josiah Schwab  
jwschwab@ucsc.edu

\* Hubble Fellow

to density, and so the central density of the ONe core when oxygen ignition occurs has been understood as the primary determinant of the final fate.

One-dimensional calculations (e.g., Nomoto & Kondo 1991; Gutierrez et al. 1996) suggested that this process led to collapse to a NS. However, it was understood that this conclusion was sensitive to the presence and efficiency of mixing processes in the star. Current models of electron-capture-initiated collapse, which have only recently begun to harness the power of multidimensional hydrodynamics codes, are extremely close to the threshold between implosion and explosion. Jones et al. (2016b) find that in some cases these objects do not implode, but instead explode, leaving behind a low mass bound remnant. Leung & Nomoto (2017) vary a variety of model parameters and find that the outcome switches between explosion and implosion within existing uncertainties.

Therefore, an important step in understanding the final fate of these objects is improving the modeling of the phase in which the WD approaches the Chandrasekhar mass. Such calculations inform the initial conditions for the collapse calculations. Current models of ECSN progenitors generally use relatively large nuclear networks (e.g., Jones et al. 2013; Takahashi et al. 2013), and so the compositions at the time of collapse are self-consistently set by the preceding stellar evolution. In contrast, AIC models have primarily used homogeneous degenerate cores where the focus is restricted to the most abundant isotopes  $^{16}\text{O}$ ,  $^{20}\text{Ne}$ , and  $^{24}\text{Mg}$  (e.g., Canal et al. 1992; Gutierrez et al. 1996; Schwab et al. 2015). Gutiérrez et al. (2005) extend this to include the effects of  $^{12}\text{C}$  and  $^{23}\text{Na}$ , which can be present with mass fractions at the percent level. Gutiérrez et al. (2005) find that  $^{12}\text{C}$  can lead to low density explosions, but that  $^{23}\text{Na}$  has little effect. Using a more accurate treatment of the relevant weak reaction rates (Paxton et al. 2015; see also Fuller et al. 1985; Toki et al. 2013; Martínez-Pinedo et al. 2014; Suzuki et al. 2016), Schwab et al. (2017a) demonstrate that Urca-process cooling due to  $^{23}\text{Na}$  has a significant effect on the thermal state of the WD.

In this paper, we revisit the role of  $^{12}\text{C}$  in the evolution of massive ONe WDs towards AIC. In Section 2, we generate a set of massive ONe WD models and characterize their chemical compositions. In Section 3, we describe how the composition profile of the WD changes during its evolution towards collapse. Guided by these results, in Section 4 we use a set of simple WD models to demonstrate the effects of  $^{12}\text{C}$ . In Section 5, we evolve our realistic WD models towards collapse. In Section 6,

we conclude and indicate areas of important remaining uncertainty in their evolution towards collapse.

## 2. COMPOSITION OF OXYGEN-NEON WDS FROM STELLAR MODELS

Super asymptotic giant branch (SAGB) stars that produce ONe WDs first produce partially degenerate CO cores. Off-center carbon ignition then occurs, leading to the formation of a convectively-bounded “flame” that propagates inward (e.g., Timmes et al. 1994). The ashes of carbon burning are dominated by  $^{16}\text{O}$  and  $^{20}\text{Ne}$  with  $^{23}\text{Na}$  and  $^{24}\text{Mg}$  also being produced at mass fractions of  $\approx 5\%$ . Some of the  $^{12}\text{C}$  can remain unburned, with the amount and its distribution within the WD varying with the mass of the star and assumptions related to the propagation of the flame (Siess 2006).

In order to produce a set of ONe WD models with self-consistent abundance profiles, we evolve a set of SAGB star models using Modules for Experiments in Stellar Astrophysics (MESA; Paxton et al. 2011, 2013, 2015, 2018). In Sections 2.1 and 2.2 we describe these models and their compositions. In Section 2.3 we compare our results to the SAGB models of Siess (2007). We note that these SAGB models are constructed within a single-star framework, though ONe WDs that undergo AIC necessarily have binary companions. Exploring how the binary evolution (though mass transfer, tides, etc.) affects the properties of the WDs that we expect to undergo AIC is an interesting avenue for future work.

### 2.1. Setup of SAGB MESA models

Farmer et al. (2015) use MESA to investigate the properties of carbon burning in SAGB stars as a function of the initial stellar mass and rotation rate as well as mixing parameters including convective overshooting. They use fine spatial and temporal resolution in order to carefully resolve the carbon flame. We therefore elect to use the MESA input files from Farmer et al. (2015) as the framework for producing ONe WDs with realistic composition profiles. We updated the Farmer et al. (2015) input files to be compatible with MESA version 9793. We then evolve models from the pre-main sequence to the SAGB and through the carbon flame phase.

We now summarize some of the key input physics and modeling assumptions made by Farmer et al. (2015) and hence adopted in our models. For complete details, we refer the reader to Farmer et al. (2015) and the MESA instrument papers (Paxton et al. 2011, 2013, 2015, 2018).

We use the MESA nuclear network `sagb_NeNa_MgAl.net` which uses 22 isotopes to cover the H, He, and C burning phases (including the pp chains and the CNO, NeNa, and MgAl cycles). Mass loss is treated via the Reimers

mass loss prescription (Reimers 1975) on the RGB with  $\eta = 0.5$  and a Bloeker mass loss prescription (Bloeker 1995) on the AGB with  $\eta = 0.05$ . Convective stability is evaluated using the Ledoux criterion. Semiconvection is included via the prescription of Langer et al. (1985) with a dimensionless efficiency factor of 0.01. Thermohaline mixing is included using the prescription of Kippenhahn et al. (1980) with a dimensionless efficiency factor of 1. Convective overshooting is implemented in MESA via an exponential decay of the convective mixing diffusion coefficient beyond the fully convective boundary (Herwig 2000). The lengthscale of this decay, and hence the extent of the overshooting region, is controlled by the dimensionless parameter  $f_{\text{ov}}$  which multiplies the local pressure scale height. When we include overshooting, we use an overshooting efficiency of  $f_{\text{ov}} = 0.016$ . Rotation in MESA uses the shellular approximation (Meynet & Maeder 1997) and is described in Paxton et al. (2013). Stellar models are given an initial solid body rotation rate at ZAMS. When we include rotation in our models, we use an initial rotation rate of 0.25 the critical rotation rate  $\omega_{\text{crit}}$ . The MESA implementation of rotation and angular momentum transport closely follows that of Heger et al. (2000) and Heger et al. (2005). Transport is treated within the diffusion approximation and considers the effects of the following processes: the dynamical shear instability (DSI), secular shear instability (SSI), EddingtonSweet circulation (ES), GoldreichSchubertFricke instability (GSF), and SpruitTaylor dynamo (ST). We do not include the effects of rotationally-enhanced mass loss or other angular momentum loss mechanisms such as magnetic braking. While many of these choices have associated uncertainties and caveats, on the whole, we believe that this produces models of SAGB stars that are broadly representative of those in the literature.

Following SAGB stars through their final phases is computationally demanding. For a recent review of some of the challenges of modeling stars in this mass range see Doherty et al. (2017). We invest the effort to carefully track the off-center carbon burning as it migrates to the center and forms the degenerate ONe core. However, difficult evolutionary phases remain before the star leaves behind a WD. One challenge comes from needing to track a large number of thermal pulses (hundreds to thousands). This would require a prohibitively large number of timesteps, so we wish to halt our models before the TP-SAGB phase.<sup>1</sup> This does mean that

the WD models that we produce have somewhat different masses than if they had been allowed to evolve through the TP-SAGB. Another challenge comes from contending with those models that experience “dredge-out” events. This occurs when the hydrogen-rich convective envelope merges with the helium-burning convective shell (e.g., Ritossa et al. 1999; Gil-Pons & Doherty 2010). This leads to a hydrogen flash as protons are mixed into regions of high temperature on the convective turnover time. During this phase, our MESA models encounter numerical difficulties and are unable to continue. Stellar evolution codes may be poor tools to follow these dredge-out events as the hydrogen burning can become sufficiently rapid that standard assumptions about mixing length theory may be unlikely to hold (Jones et al. 2016a).

In summary, we cannot simply allow our MESA SAGB models to naturally evolve, eject their envelopes, and produce WDs. Since the challenges occur after completion of the carbon flame phase (and thus after the core composition is done evolving), we decide to manually halt the evolution and eject the envelope.<sup>2</sup> We develop a simple, *ad hoc* procedure that halts the models before the onset of thermal pulses or dredge-out.

We stop the evolution and eject the envelope once two conditions are met simultaneously. First, we check if the highest temperature in the region of the star where the energy generation rate is dominated by CNO-cycle hydrogen burning is greater than roughly  $3 \times 10^7$  K. This condition is naturally triggered as the hydrogen-burning shell develops before the first thermal pulse and is necessarily triggered before high-temperature proton ingestion can lead to numerical difficulties. Second, we check that the CO core mass and the ONe core mass are within 10% of each other. This condition ensures that we do not stop the evolution before the ONe core has finished forming. At this point, we remove the envelope using an artificially-enhanced stellar wind with  $\dot{M} \sim 10^{-2} M_{\odot} \text{ yr}^{-1}$ . We turn off nuclear burning during this phase for numerical simplicity. After the envelope has been removed we are left with a hot ONe WD model with a thin hydrogen and helium envelope.

Our goal is to produce a set of WD models that have a range of qualitatively different chemical profiles. Therefore, like Farmer et al. (2015), we vary a handful of stellar parameters including initial mass, rotation at the

<sup>1</sup> Stopping before the thermal pulses (as opposed to stopping after a few thermal pulses) also proved to make it simpler to artificially remove the envelope.

<sup>2</sup> We note that in many evolutionary scenarios leading to AIC, the envelopes of the progenitor stars have already been stripped through binary interaction and thus never have a TP-SAGB (e.g., Tauris et al. 2015).

zero-age main sequence (ZAMS), and the location and strength of convective overshooting.

We run a set of non-rotating models without any convective overshoot (series NRNO). We run a set of models (series RO) with the fiducial rotation and overshooting parameters adopted by [Farmer et al. \(2015\)](#), which includes overshoot at all convective boundaries. The propagation of the carbon flame, and therefore the subsequent chemical profile, is sensitive to the treatment of mixing at the convective boundary near the flame ([Siess 2009](#); [Denissenkov et al. 2013](#)). To explore this effect, we also run a set of rotating models (series RMO) with an overshooting treatment where mixing below convective regions associated with carbon burning does not occur. This corresponds to the MESA options

```
overshoot_f_below_burn_z_shell = 0.000
overshoot_f0_below_burn_z_shell = 0.000
```

This choice is motivated by the findings of [Lecoanet et al. \(2016\)](#) who performed idealized hydrodynamic simulations of a carbon flame and found that little mixing occurs at this interface as convective plumes were not able to penetrate into the carbon flame.

## 2.2. Results of SAGB MESA models

We produced a total of 12 WD models. These models and their identifiers are listed in Table 1 together with the key parameters including initial mass, rotation at ZAMS, and convective overshooting. All but one model produce massive ONe WDs. Model 5 produces a hybrid CO-ONe WD.

Convective overshooting and rotation can have large effects on the chemical profile of the WD and especially that of  $^{12}\text{C}$ . Figure 1 shows the carbon profiles in our models; each panel compares different initial masses within the same model series. Broadly, models from more massive stars have less carbon than those from lower mass stars.<sup>3</sup> This trend is set as models transition from flames that fail to reach the center (leaving lots of unburned carbon) at lower mass to central carbon ignitions (with almost complete carbon burning) at higher mass. The detailed behavior in between these extremes is complex, with a mixture of carbon flames and flashes (see e.g., Figure 3 in [Farmer et al. 2015](#)). This trend is particularly pronounced in the models that include overshooting (left and center panels). Models 1-8 from series RMO and RO have carbon depletion especially at

larger radii while models 9-12 from series NRNO have comparatively homogeneous carbon profiles.

Stellar models that exhibit efficient convective overshooting below the carbon flame tend to extinguish the carbon flames earlier resulting in an increased abundance of carbon in the core. This effect is clearly visible in the left and center panels of Figure 1. The profiles of series RO and series RMO, which differ only by their assumption about mixing below the carbon flame, have similar carbon profiles in the outer half of the cores. However, series RO has systematically higher carbon abundances in the inner regions than series RMO. We find that all 12 WD models exhibit qualitative differences in their carbon profiles depending on their initial masses and modeling assumptions.

## 2.3. Comparison to Siess Models

[Siess \(2007\)](#) constructed SAGB models using the stellar evolution code STAREVOL. These models do not take into account the effects of rotation. Like our MESA models, they use a decaying exponential treatment for convective overshooting with the same value of  $f_{\text{ov}} = 0.016$ , though this is only applied at the edge of the convective core. We compare our models with their solar metallicity ( $Z = 0.02$ ) models that include convective overshooting.

Figure 2 shows the central  $^{12}\text{C}$  abundance at the end of carbon burning as a function of initial mass. The models from [Siess \(2007\)](#) are shown as gray squares. Models with higher initial masses have lower central carbon fractions. Our MESA models exhibit similar trends. Our models are not directly comparable to the Siess models at fixed initial mass because the different assumptions about rotation and overshooting imply a different mapping between initial mass and core mass. However, these independent sets of SAGB models display the same feature that stars in this transition mass range show a broad range of central carbon mass fractions ranging from tenths of a percent to tens of percent.

Figure 2 also illustrates the sensitivity of the central carbon fraction to convective overshooting below regions associated with carbon burning. The series RO models have central carbon mass fractions up to a factor of 10 greater than those in series RMO at fixed initial mass; again, the only difference between these models is the overshooting parameter at the lower boundary of the convection zone immediately above the carbon flame.

## 3. HOMOGENIZATION DURING WD COOLING

In order for the ONe WD to evolve towards collapse, it must eventually accrete from a companion. This interaction is unlikely to begin immediately after the formation

<sup>3</sup> This is why  $^{12}\text{C}$  is generally not important in single-star models for ECSNe which are necessarily more massive than those that produce ONe WDs. For example, after the end of core carbon burning, the ECSN progenitor model of [Takahashi et al. \(2013\)](#) has a  $^{12}\text{C}$  mass fraction  $\approx 10^{-3}$ .

**Table 1.** Summary of ONe WD models. Models in a series are evolved with an identical treatment of rotation and convective overshooting. The left part of the table shows the model identifiers. The middle part shows initial conditions and model parameters. The right part shows key properties of the formed WDs. Note that the WD progenitor models had their evolution artificially truncated before the TP-SAGB. If they were allowed to evolve through the TP-SAGB, the mass of the WD might be somewhat different (depending on the efficiency of third dredge-up).

Series	Model	Initial Mass	Rotation	Overshooting	WD Model Mass	Central $^{12}\text{C}$ [%]	
		$[M_{\odot}]$	$[\omega/\omega_{\text{crit}}]$	$(f_{\text{ov}})$	Mass $[M_{\odot}]$	pre-cool	post-cool
RMO	1	7.2	0.25	0.016 / 0.000	1.06	6.99	2.69
	2	7.6			1.18	0.98	0.69
	3	8.0			1.28	0.22	0.18
	4	8.4			1.34	0.25	0.07
RO	5	7.2	0.25	0.016	1.08	32.72	16.30
	6	7.6			1.17	15.76	2.89
	7	8.0			1.28	3.94	1.02
	8	8.4			1.34	0.31	0.09
NRNO	9	9.5	0.00	0.000	1.01	2.46	2.65
	10	10.0			1.09	4.23	1.64
	11	10.5			1.14	2.16	1.19
	12	11.0			1.19	0.68	0.63

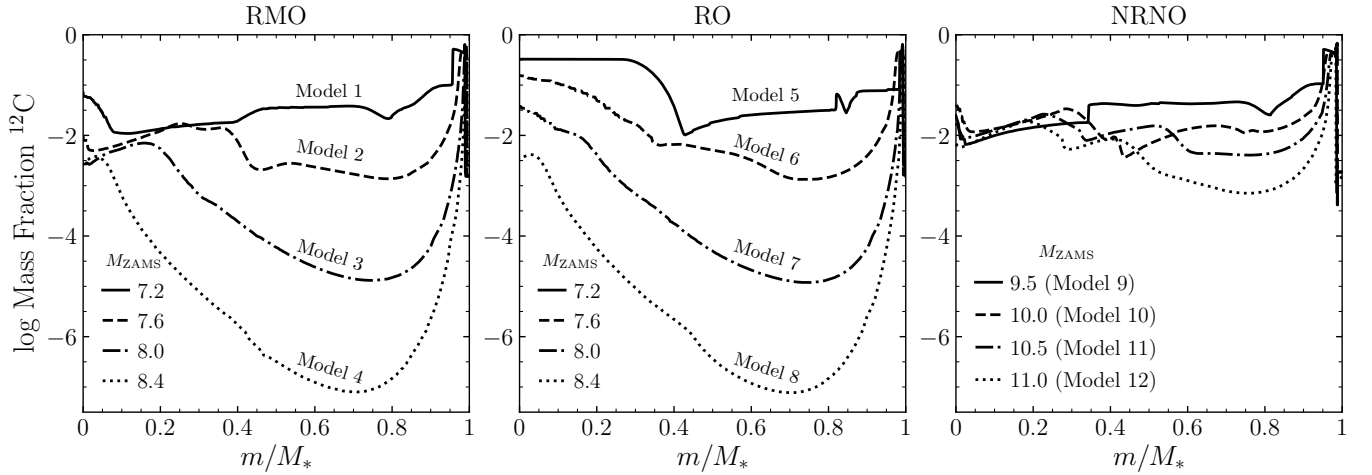


**Figure 1.** Carbon profiles as a function of normalized mass coordinate for all 12 WD models (before cooling). Each panel shows a group of WD models from stars of different initial (ZAMS) masses that use identical stellar modeling parameters. The initial conditions and parameters for each model are indicated in Table 1.

of the WD, but must instead wait for the companion star to evolve and fill its Roche lobe. Therefore, our modeling assumes that after formation there is a phase of evolution in which the WD does not interact with its companion and simply cools as an effectively single object.

As a WD cools and approaches an isothermal configuration, mixing can smooth out compositional gradients

in the WD interior.<sup>4</sup> Often in the literature this process is referred to as “rehomogenization”—framed as Rayleigh-Taylor instabilities smoothing regions with negative molecular weight gradients—and is often as-

<sup>4</sup> While we describe these mixing processes as occurring during WD cooling, in models that self-consistently follow the evolution through the TP-SAGB, they may have already begun to act during that phase.



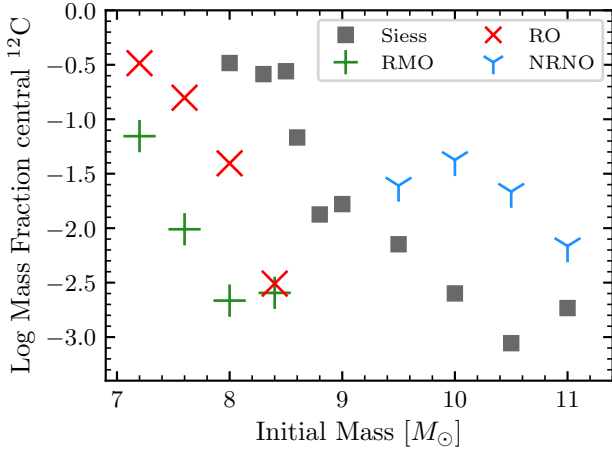


**Figure 2.** Central carbon abundance in SAGB models as a function of initial mass. Our MESA models (colored symbols) are split into three different groups with differing stellar controls including initial mass, rotation, and overshooting (see Table 1). For comparison, the SAGB models of Siess (2007) are shown as the gray squares.

sumed to occur quasi-instantaneously (e.g., Althaus et al. 2007; Camisassa et al. 2018). However, more formally, the presence of a destabilizing composition gradient leads to mixing via thermocompositional convection. Depending on the magnitude of the stabilizing temperature gradient, this can take the form of overturning convection or double-diffusive fingering (thermohaline) convection. This distinction is important as these different processes occur over different timescales.

In CO WDs, the evolutionary effects of this kind of mixing are generally minor. However in hybrid CO-ONe WDs, where an ONe mantle overlays a CO core, such mixing is of critical importance as it will destroy the stratified core-mantle structure on a timescale significantly shorter than the likely timescale for the WD to grow to the Chandrasekhar mass (Brooks et al. 2017). The complex carbon profiles at formation in our ONe WD models (see Section 2.2) will similarly be affected by these mixing processes and this can substantially alter the central carbon fraction.

In order to illustrate the effects of the mixing processes, we show the evolution of our WD model 2 (see Table 1) during cooling. Figure 3 shows the model evolving assuming no thermohaline mixing occurs while Figure 4 shows the model evolving including thermohaline mixing. The lower panels of these plots show the electron fraction ( $Y_e$ ): as the temperature becomes isothermal, convection alone will leave behind the neutrally buoyant  $Y_e$  profile while the addition of thermohaline mixing leads to a flat  $Y_e$  profile. The upper panels show the effects that mixing has on the  $^{12}\text{C}$  abundance. Fig-

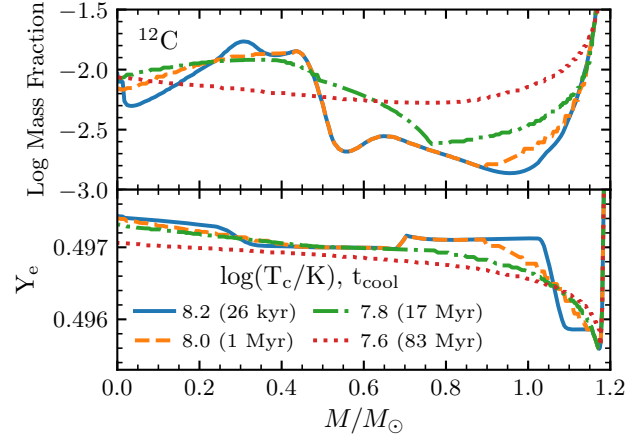


**Figure 3.** Evolution of the chemical profiles during WD cooling *without* thermohaline mixing. The upper panel shows the  $^{12}\text{C}$  mass fraction and the lower panel shows  $Y_e$ , both as a function of the Lagrangian mass coordinate. Profiles are shown at a sequence of central temperatures; the time to reach the given temperature is indicated in parenthesis.

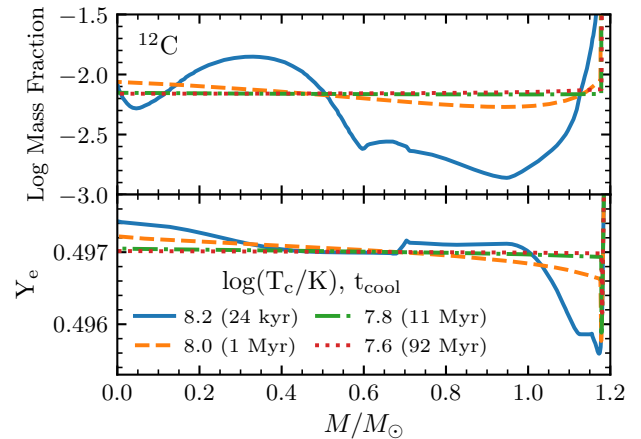


**Figure 4.** Evolution of the chemical profiles during WD cooling *with* thermohaline mixing (cf. Figure 3).

ure 3 shows that without thermohaline mixing, a significant gradient in the  $^{12}\text{C}$  profile and  $Y_e$  persists after 80 Myr. In contrast, the WD model with thermohaline mixing shown in Figure 4 has already reached a similar level of homogenization after 1 Myr and has almost completely homogeneous  $^{12}\text{C}$  and  $Y_e$  profiles after only 11 Myr. This behavior is similar to what was found in Brooks et al. (2017).

Moving forward, all of our WD models are evolved using thermohaline mixing, as this is an expected physical effect. We do not include the effects of phase separation at crystallization which may further affect the central abundances (Segretain & Chabrier 1993); such capabil-

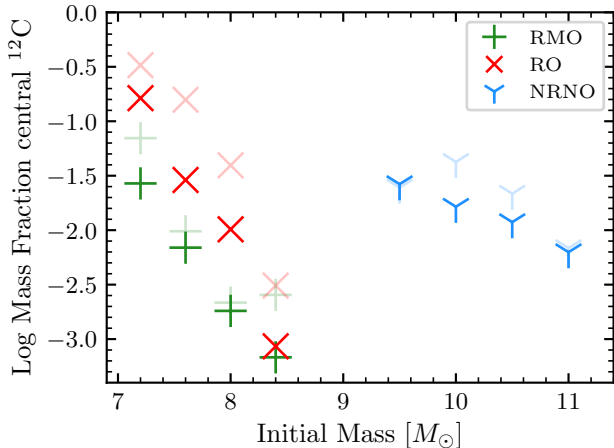


**Figure 5.** Central carbon abundance as a function of the initial stellar mass after the WD models have cooled for  $\approx 100$  Myr. Translucent points indicate central carbon abundances prior to cooling (same as Figure 2).

ities are not presently included in *MESA*. Since  $^{12}\text{C}$  has the lowest charge of the isotopes present, the effect of phase separation would likely be to reduce the central carbon abundance.

After  $\approx 100$  Myrs of cooling, all our WD models exhibit effectively homogeneous interior chemical profiles. Figure 5 shows the central mass fractions at this time; this value now reflects the abundance throughout the interior. The pale symbols show the mass fractions before cooling, illustrating that the central abundance of isotopes like  $^{12}\text{C}$  can change by a factor of a few. (The values pre- and post-cooling are also reported in Table 1.) In Section 2, we showed that varying initial mass, convective overshoot, and rotation produced ONe WDs having chemical profiles with qualitatively different shapes, but here we have shown that those differences are subsequently erased. However, Figure 5 shows that the overall range of central carbon abundance across models persists.

#### 4. EFFECTS OF RESIDUAL CARBON

In Sections 2 and 3, we showed that ONe WD models from SAGB star evolution using *MESA* had residual  $^{12}\text{C}$  mass fractions  $X_{12} \approx 10^{-3} - 10^{-1}$ . In this section, we will outline the role of  $^{12}\text{C}$  in the evolution of the WD towards collapse. Similarly, Gutiérrez et al. (2005) evolve a set of ONe WD models with parameterized  $^{12}\text{C}$  mass fractions in the range  $X_{12} = 0.01 - 0.06$ , motivated by the unburnt carbon in SAGB models (Dominguez et al. 1993; Ritossa et al. 1996; Gil-Pons & García-Berro 2001, 2002). They find that that models with relatively small  $^{12}\text{C}$  abundances ( $X_{12} \gtrsim 0.015$ ) can allow for ignition at densities  $\sim 10^9 \text{ g cm}^{-3}$ . Ignition at these low densities

seems likely lead to disruption of the star. Indeed, if carbon burning occurs before the exothermic electron captures, the evolution will be more analogous to the simmering phase experienced by near-Chandrasekhar mass CO WDs in which carbon burning leads to the development and growth of a large central convection zone (e.g., Lesaffre et al. 2006; Piro & Chang 2008). However, as we will demonstrate shortly, the presence of Urca-process cooling due to  $^{23}\text{Na}$  makes it unlikely that carbon ignition occurs in advance of the exothermic electron captures on  $^{24}\text{Mg}$  and  $^{24}\text{Na}$ .

##### 4.1. Carbon Ignition and Electron Captures

The models in Gutiérrez et al. (2005) start with central conditions  $\rho_c = 10^9 \text{ g cm}^{-3}$  and  $T_c = 2 \times 10^8 \text{ K}$ . From their Figure 3, it appears that these models almost immediately begin carbon burning. For lower carbon mass fractions, the carbon-burning runaway takes slightly longer, allowing additional compression to occur during the temperature increase. The lowest carbon mass fraction model ( $X_{12} = 0.01$ ) appears to run out of fuel before reaching temperatures  $\gtrsim 10^9 \text{ K}$  and then subsequently rejoins the compression-driven evolution towards higher density and the eventual  $^{20}\text{Ne}$  electron captures that is characteristic of their carbon-free models.

The fact that the models of Gutiérrez et al. (2005) appear to be burning carbon at or near their initial central conditions is puzzling. Figure 4 of Gasques et al. (2005) shows ignition lines (defined as where the energy generation rate is equal to the thermal neutrino losses) and burning timescales for pure carbon that cover the relevant range of densities and temperatures. The initial central conditions from Gutiérrez et al. (2005) are well below even a burning timescale of order a Hubble time.

Figure 6 shows the carbon ignition lines for a range of carbon mass fractions. These are evaluated with the same input physics as our subsequent *MESA* models. We use the carbon burning rate from Caughlan & Fowler (1988) and the “extended” screening treatment in *MESA* as described in Paxton et al. (2011). This combines the results of Graboske et al. (1973) in the weak regime and Alastuey & Jancovici (1978) with plasma parameters from Itoh et al. (1979) in the strong regime. The neutrino loss rates are calculated via the fitting formulae of Itoh et al. (1996). For comparison, the solid grey line shows the *MESA* implementation of the rate given by Gasques et al. (2005) for pure carbon<sup>5</sup> ( $X_{12} = 1.0$ ). At

<sup>5</sup> The extension of these results to multicomponent plasmas and hence smaller carbon mass fractions is given by Yakovlev et al. (2006), but this is not presently implemented in *MESA*.

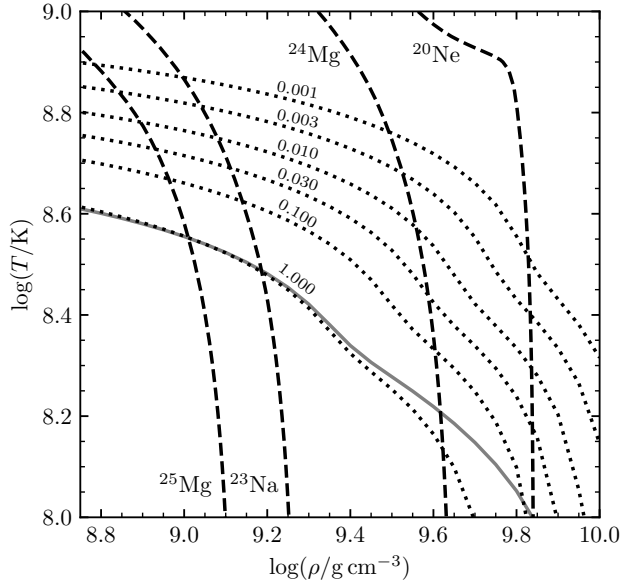


**Figure 6.** Critical lines for carbon burning and electron captures. The dotted lines show the carbon ignition curves for the input physics adopted in our MESA models, labeled by carbon mass fraction. The solid gray line shows the ignition curve for pure carbon using the rate from Gasques et al. (2005). The dashed lines show where the indicated isotope has an electron capture timescale of  $10^4$  yr.

low temperature (roughly in the regime where  $T$  is below the ion plasma temperature), these ignition curves disagree, reflecting differences in the screening treatment. Figure 4 of Gasques et al. (2005) shows the theoretical uncertainty associated with the ignition curves in this regime; the pure carbon MESA ignition curve in Figure 6 lies within that range.

Figure 6 also indicates where the key weak reactions will become important. The dashed lines show where the electron capture timescale for each of  $^{25}\text{Mg}$ ,  $^{23}\text{Na}$ ,  $^{24}\text{Mg}$ , and  $^{20}\text{Ne}$  is equal to a characteristic compression timescale of  $10^4$  yr (Schwab et al. 2015), with more rapid electron captures occurring to the right of the line. These curves were evaluated using the rate tabulations of Suzuki et al. (2016) assuming  $Y_e = 0.5$ .

#### 4.2. Simple MESA Models

In order to illustrate the potential role of carbon, we follow the approach of Schwab et al. (2015, 2017a) by constructing quasi-homogeneous WD models with parameterized abundances. This provides a simple way to isolate the effects of  $^{12}\text{C}$ . In Section 5 we will apply this understanding to the more realistic WD models described in previous sections. The calculations shown in this section use MESA version 10108. All input files will be made publicly available at <http://mesastar.org>.

**Table 2.** The set of compositions used in our MESA models. Each composition is referenced in the text by the identifier listed in the top row. Each column lists the mass fractions of the isotopes that were included. Dashes indicate that a particular isotope was not included. A range of  $^{12}\text{C}$  mass fractions were considered; the  $^{20}\text{Ne}$  mass fraction was chosen to ensure the mass fractions sum to unity.

Isotope	SQB15C	SBQ17C
$^{12}\text{C}$	0.0 - 0.1	0.0 - 0.1
$^{16}\text{O}$	0.50	0.50
$^{20}\text{Ne}$	remainder	remainder
$^{23}\text{Na}$	—	0.05
$^{24}\text{Mg}$	0.05	0.05
$^{25}\text{Mg}$	—	0.01

We first create a pre-main sequence star of  $1.0 M_\odot$  with a solar composition. We select this as a starting point because a high-entropy model is more amenable to our relaxation procedure than a highly degenerate WD model. During these relaxation phases, we disable nuclear reactions. We evolve until the model reaches a central density of  $\log(\rho_c/\text{g cm}^{-3}) = 4$  and then we relax its composition to one of the compositions indicated in Table 2. These are the fiducial compositions from Schwab et al. (2015, 2017a) plus a variable amount of carbon. We continue the evolution, with the model cooling and contracting, until it reaches a central density of  $\log(\rho_c/\text{g cm}^{-3}) = 7$ . We then have the models accrete a 50/50 oxygen-neon mixture<sup>6</sup> at a rate  $10^{-6} M_\odot \text{ yr}^{-1}$  until the WD has reached  $\log(\rho_c/\text{g cm}^{-3}) = 8.6$ . This value is selected to be below the density at which electron captures on the isotopes present in the initial composition will first occur. This procedure creates near-Chandrasekhar mass WD models with homogeneous inner regions of the desired compositions.

We then take these models and continue letting them accrete at  $10^{-6} M_\odot \text{ yr}^{-1}$ . This choice represents an accretion rate that is roughly characteristic of any near-Chandrasekhar WD accretor stably burning hydrogen or helium (e.g., Wolf et al. 2013; Brooks et al. 2016). The long period of accretion in these models means that the memory of their initial central temperatures are erased as the models come into a balance where the compressional heating balances neutrino losses (Paczynski 1971; Schwab et al. 2015; Brooks et al. 2016). However, this does imply that the temperature of these models is set by our choice of accretion rate. We evolve until the

<sup>6</sup> We accrete material that is free of hydrogen, helium and carbon in order to avoid the complications associated with following the nuclear burning on the surface of the WD.



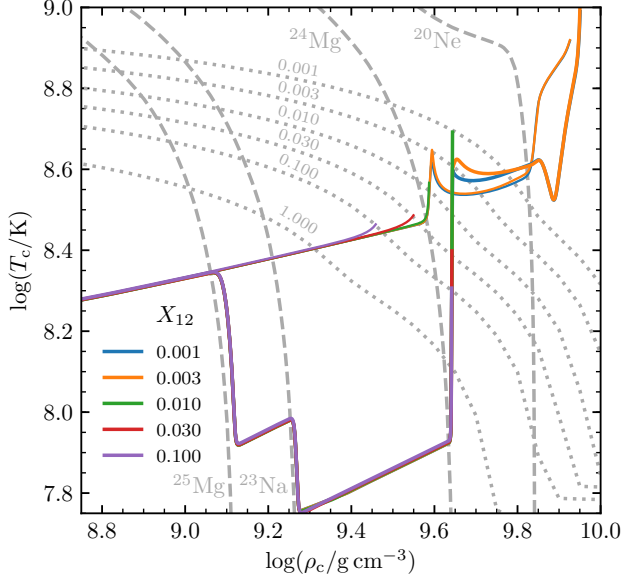


**Figure 7.** Evolution of simplified WD models with a range of carbon fractions. The thin lines show models without Urca cooling (composition SQB15C); the thick lines show models with Urca-process cooling (composition SBQ17C). The light grey lines in the background are the same as those in Figure 6. Models are halted when the energy release from carbon burning locally exceeds thermal neutrino losses.

model experiences carbon ignition (defined as the energy release from carbon burning locally exceeding thermal neutrino losses). We note that some models, in particular those with carbon fractions  $\lesssim 0.01$ , may evolve beyond the carbon ignition lines corresponding to their initial carbon abundances. This is because by the time an evolutionary model reaches the temperature and density of the ignition curve corresponding to its initial carbon abundance, some of the carbon can have already been consumed.

Schwab et al. (2017a) demonstrated that models that experience electron captures after significant Urca-process cooling has occurred can develop convectively-unstable regions near the electron capture front. Proper modeling of this convection likely requires both theoretical and numerical progress and remains an important open question. We discuss the difficulties of evolving MESA models in this phase more specifically in Section 5. To circumvent these issues, we artificially suppress the action of convection in the MESA models using the control `mlt_option = 'none'`. This is an important caveat that applies to the evolutionary tracks shown in Figure 7 after  $^{24}\text{Mg}$  electron captures ( $\log(\rho/\text{g cm}^{-3}) \gtrsim 9.6$ ). Nonetheless, these models still provide insight into when carbon burning first begins to affect the evolution.

Figure 7 shows the evolution of the central temperature and density in the models. The thin lines show the results of models with the SQB15C composition, which do not include Urca-process cooling since there is no  $^{23}\text{Na}$  or  $^{25}\text{Mg}$ . These models are less physically realistic, but we show them primarily for comparison with the results of Gutiérrez et al. (2005). Models with  $X_{12} \gtrsim 0.02$  experience carbon ignition at densities below where electron captures on  $^{24}\text{Mg}$  would occur. Energetically, it requires burning approximately  $0.02 M_{\odot}$  of carbon to heat the WD to the conditions for dynamical burning (Piro & Bildsten 2008). Therefore, since these models have roughly that much carbon, if we continued their evolution they may be able to reach the conditions for thermonuclear explosions. Note that the  $X_{12} = 0.1$  model is similar to what one would expect from a fully-mixed hybrid CO-ONe WD. Models with very low carbon abundances  $X_{12} \lesssim 0.003$  evolve much like carbon-free models; the thin orange and blue lines are nearly identical and continue until oxygen ignition. Intermediate abundance models with  $0.003 \lesssim X_{12} \lesssim 0.02$  experience carbon ignition as a result of the  $A = 24$  electron captures. This range encompasses the carbon fractions in many of the ONe WD models shown in Section 3.

However, the presence of Urca-process cooling changes this picture, causing models across a range of compositions and accretion rates to reach  $T_c \lesssim 10^8 \text{ K}$  (see Equation 15 in Schwab et al. 2017a). The thick lines in Figure 7 show the results of models with composition SBQ17C; the presence of  $^{23}\text{Na}$  and  $^{25}\text{Mg}$  leads to significant cooling. Models that experience this cooling will therefore almost certainly reach the  $^{24}\text{Mg}$  electron captures before igniting carbon. Models with very low carbon abundances  $X_{12} \lesssim 0.003$  evolve much like carbon-free models (though again, we note that these models do develop convectively unstable regions that are artificially not allowed to mix). Models with  $X_{12} \gtrsim 0.01$  experience carbon ignition as a direct result of the  $A = 24$  electron captures.

Stellar models indicate significant abundances of the odd mass number isotopes (in particular  $^{23}\text{Na}$ ) that are responsible for the Urca-process cooling. Thus the SBQ17C models are the ones that should guide our understanding of WDs with self-consistently set compositions. Urca-process cooling prevents carbon ignitions from occurring in advance of the exothermic electron captures on  $^{24}\text{Mg}$ . The SBQ17C models do show carbon ignition triggered by the  $A = 24$  electron captures above a critical carbon fraction of around 1 per cent by mass. Since this is within the range seen in our self-consistent stellar models of ONe WDs, this is an indica-

tor that carbon may play an important role in at least some systems.

## 5. EVOLUTION TO COLLAPSE

In this section, we continue the schematic binary evolution of the WD models produced in Sections 2 and 3 and examine the role of carbon in the evolution towards their final fates.

### 5.1. Setup of accreting WD models

In the overall evolutionary scenario for AIC, the ONe WD will stop cooling once it begins accreting from its companion via Roche lobe overflow. This can be achieved through expansion of the secondary driven by stellar evolution processes or a shrinking of the orbit through angular momentum losses. Either process results in a massive WD accreting material.

We model the effects of accretion from a companion by adding a constant accretion rate of  $^{16}\text{O}$ . We again select a rate of  $10^{-6} M_{\odot} \text{ yr}^{-1}$  as roughly characteristic of any near-Chandrasekhar WD accretor stably burning hydrogen or helium. Accreting oxygen simplifies the models as it avoids having to follow the numerically challenging hydrogen, helium, or carbon flashes that could occur during the accretion process. We turn rotation off on all models to avoid numerical problems with angular momentum transport in the WD. This is consistent with past work that has primarily studied non-rotating WDs.

We use a version of the original nuclear network `sagb_NeNa_MgAl.net` modified to add the isotopes  $^{19}\text{O}$ ,  $^{20}\text{O}$ ,  $^{20}\text{F}$ ,  $^{21}\text{F}$ ,  $^{23}\text{F}$ ,  $^{23}\text{Ne}$ ,  $^{24}\text{Ne}$ ,  $^{24}\text{Na}$ ,  $^{25}\text{Ne}$ ,  $^{27}\text{Na}$ , and  $^{27}\text{Mg}$  and the weak reactions that link them to the isotopes originally present in our network. We use the reaction rate tables from Suzuki et al. (2016) which are specifically calculated for the conditions in high-density ONe cores. We adopt EOS options<sup>7</sup> and spatial/temporal resolution controls similar to those of Schwab et al. (2017a), as it is demonstrated that those choices lead to numerically converged models (see their Appendix B).

### 5.2. Model evolution

We show the evolution of the central density and temperature of a subset of our models in Figure 8. In particular, we select models 2 and 6 from Table 1. These models both descend from  $7.6 M_{\odot}$  ZAMS models, with

<sup>7</sup> Schwab et al. (2017a) include all isotopes in the nuclear network in the PC (Potekhin & Chabrier 2000) EOS calculations by using the control `mass_fraction_limit_for_PC = 0d0`. In MESA r9793 doing so with networks including neutrons causes the program to halt unexpectedly. We backport the one-line fix from MESA commit r10361 to our version.

the only difference between them being the efficiency of overshooting associated with the carbon flame. These produce similar WD models that differ mainly in their carbon abundance; model 2 and model 6 have central carbon mass fractions of 0.007 and 0.03 respectively.

Compared to the toy models in Section 4, these models begin somewhat cooler. This is because the toy models had been steadily accreting since they were much lower mass and had reached a balance between compressional heating and neutrino cooling (Paczynski 1971). In contrast, our realistic ONe WD models had already cooled below this temperature, and being initially more massive, have not accreted for long enough to reheat.

The annotations on the lower part of the figure indicate the location of key weak reactions. We see some difference from the toy models shown in Figure 7. Mildly exothermic captures on  $^{27}\text{Al}$  occur; this species is not included in our toy models. The Urca-process cooling due to  $^{25}\text{Mg}$  is less than in the toy models, due both to the initially lower temperature and the lower abundance of this isotope. The cooling from  $^{23}\text{Na}$  is more dramatic, though the small glitch near the end of cooling is an artifact of the reaction rate tables and does correspond to slightly too little cooling (see Appendix D in Schwab et al. 2017a). The separation (in density) of the  $^{24}\text{Mg}$  and  $^{24}\text{Na}$  electron captures is caused by different assumed strengths of the (currently unmeasured) non-unique second forbidden transitions (see Section 5 in Schwab et al. 2017a).

All model tracks are similar up until the electron captures on  $^{24}\text{Na}$ . The heating from these is sufficient to ignite carbon. We are unable to evolve the models including the effects of convection beyond this point. By artificially suppressing convection, we are able to continue their evolution. These tracks are marked “no convection” in Figure 8. Subsequently, the difference between the two model tracks is apparent, with the a bifurcation reflecting the difference in the carbon abundance. The low carbon fraction model 2 continues to high density while the low carbon fraction model 6 experiences a relatively low density carbon-assisted oxygen ignition.

### 5.3. Convective Instability and Carbon Burning

Both in Section 4 and in this section, we encountered numerical difficulties when convective regions developed in the regions of the star undergoing electron-capture reactions. We circumvented this problem by artificially turning off convection. The further evolution of the models is thus unphysical, though hopefully remains schematically useful.

To understand why it is difficult to evolve the models beyond this point, it is first important to recall why

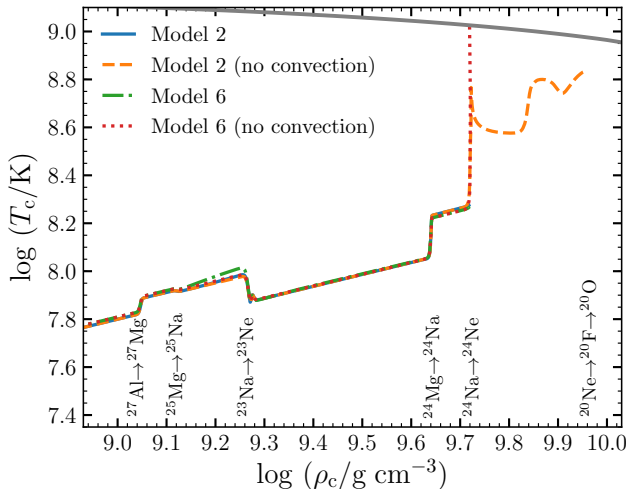


**Figure 8.** Central evolution of a lower carbon fraction model (model 2,  $X_{12} \approx 0.007$ ) and a higher carbon fraction model (model 6,  $X_{12} \approx 0.03$ ). Annotations indicate the densities at which key weak reactions occur. We show models evolved normally (which terminate at the onset of electron captures on  $^{24}\text{Na}$ ) and models evolved without convection (which terminate roughly at oxygen ignition). The gray line is the oxygen ignition curve.

these models become convective. The onset of exothermic electron captures leads to a strongly destabilizing temperature gradient. However, this is locally accompanied by the development of a strongly stabilizing composition (electron fraction) gradient. When using the Ledoux criterion, this can lead to overall convective stability (e.g., Miyaji & Nomoto 1987; Schwab et al. 2015). The crossed temperature and composition gradients mean that this region is unstable to double diffusive convection, though this process is thought to operate too slowly to have a significant effect given the short evolutionary timescale. When including the effects of Urca-process cooling, the models of Schwab et al. (2017a) became convectively unstable because thermal conduction causes a more rapid spread of the thermal gradient and leads to a situation in which the thermal and compositional gradients can no longer balance locally because their spatial extents are no longer well-matched. We emphasize that the development of these convective regions is unrelated to the presence of  $^{12}\text{C}$  and occurs even in carbon-free models.

However, once the exothermic electron captures raise the temperature enough for carbon burning to begin, its energy release can further contribute to convective instability.<sup>8</sup> The development of a convective core has

important consequences in the overall evolution of the star. Most importantly, it distributes the entropy generated by continued carbon burning and exothermic electron captures over a larger mass. This has been shown to lead to oxygen ignition at higher densities (relative to convectively stable models), favoring collapse to an NS (Miyaji et al. 1980; Miyaji & Nomoto 1987).

The numerical difficulties that occur once a convection zone develops are essentially the same as those encountered in previous work, thus we briefly recapitulate the discussion from Section 6 of Schwab et al. (2017a).

When using MLT in MESA, cells that are convective have roughly the adiabatic temperature gradient while non-convective cells have the radiative temperature gradient. Therefore, when cells change between convective and radiative, they change the overall temperature profile and in turn, this can alter the convective stability of neighboring cells. (This is further complicated by the fact that the sub-threshold electron-capture reaction rates are exponentially sensitive to temperature.) As MESA iterates to find the solution to its equations, convective boundaries change location iteration-to-iteration and the solver fails to converge.

It is clear that regions become convectively unstable, but an understanding of how and whether these convective regions grow remains an outstanding problem. If a long-lived central convection zone does form, matters are further complicated as this allows for the operation of the convective Urca process (Paczynski 1973). This continues to be difficult to model in stellar evolution codes (e.g., Lesaffre et al. 2005) and current versions of MESA produce physically inconsistent results during such phases (Schwab et al. 2017b).

The choice to artificially suppress convection corresponds to the assumption that these convective regions do not grow. The evolution of our “no convection” models will be roughly accurate only if the energy and composition changes from nuclear reactions remain approximately local. In this case, the presence of carbon leads to ignition at a factor of  $\approx 2$  lower density than in the carbon-free case. In the case that a large convective core does form (invalidating our local treatment), it seems clear that this leads to higher density oxygen

carbon-burning products can occur at these densities. Since these electron captures are super-threshold they also deposit additional thermal energy. In the standard CO WD simmering case, the reactions have been carefully worked out by Piro & Bildsten (2008), Chamulak et al. (2008), and Förster et al. (2010). However, in the ONe WD case the  $^{12}\text{C}$  abundances are lower and the  $^{23}\text{Na} / ^{23}\text{Ne}$  abundances are higher. This means that the protons and  $\alpha$  particles produced in carbon burning might go through somewhat different pathways than in the standard simmering case.

<sup>8</sup> The heating from carbon burning is accompanied by some stabilizing change in composition, as immediate electron captures on

ignition than in a case without a convective core; in the carbon-free models of [Gutierrez et al. \(1996\)](#), non-convective models ignite at  $\log(\rho_c/\text{g cm}^{-3}) \approx 10$  with ignition in convective cores occurring at a central density a factor of  $\approx 2$  higher. However, the presence of carbon is likely to reduce the density relative to a carbon-free model, as the additional heating source means that fewer electron captures are required. Since we cannot follow the models through a convective Urca phase, we are unable to reliably estimate the size of this shift.

## 6. CONCLUSIONS

We have explored the role that residual  $^{12}\text{C}$  present in ONe WDs can play during their evolution towards AIC. We used **MESA** to produce 12 ONe WD models with chemical abundance profiles self-consistently generated via stellar evolution models of SAGB stars. We explored the range of  $^{12}\text{C}$  expected for different initial masses and showed its dependence on assumptions about rotation and convective overshooting (Figure 2). Our results were consistent with previous work performed using an independent stellar evolution code ([Siess 2007](#)).

While the carbon profiles at the time of WD formation were complex and varied, we showed that after  $\approx 100$  Myr of cooling the individual interior chemical profiles become nearly spatially uniform due to the effects of convection and thermohaline mixing. We typically expect WDs on the way to AIC to cool post-formation, as time is required for their binary companion to evolve and donate sufficient material. Post-cooling, a significant spread in central carbon abundances remains, with  $^{12}\text{C}$  mass fractions ranging from 0.1 to 10 per cent (Figure 5).

We then construct simple homogeneous ONe WD models with varying carbon fractions and allow them to grow via accretion. This allows us to map out the effects of the  $^{12}\text{C}$  in a controlled way. In contrast to [Gutiérrez et al. \(2005\)](#), we did not find the presence of low-density carbon ignition. Instead, we find that the occurrence of Urca-process cooling implies that models are unlikely to reach carbon ignition before  $^{24}\text{Mg}$  electron captures begin around  $\log(\rho_c/\text{g cm}^{-3}) \approx 9.6$ . We find that models with very low carbon abundances (mass fraction  $\lesssim 0.003$ ) evolve similarly to carbon-free models whereas models with higher carbon abundances (mass fraction  $\gtrsim 0.01$ ) ignite carbon burning during the electron captures. This change in behavior happens within the range of carbon fractions found in our more realistic ONe WD models.

Ultimately, the goal of studies such as this one is to advance our understanding of the final fates of accreting ONe WDs that approach the Chandrasekhar mass. A

key indicator of the likely outcome is the central density at the time of thermonuclear oxygen ignition. The exact line between explosion and collapse has not been firmly delineated, but seems to lie around  $\log(\rho_c/\text{g cm}^{-3}) \approx 9.9$  (e.g., [Timmes & Woosley 1992](#); [Leung & Nomoto 2017](#)). In the case of explosion, the models of [Jones et al. \(2016b\)](#) leave behind a low mass bound remnant. Intriguingly, several WDs with low masses and peculiar compositions have recently been discovered ([Gänsicke et al. 2010](#); [Kepler et al. 2016](#); [Vennes et al. 2017](#); [Raddi et al. 2018](#)). Understanding the connection between these objects and AIC is an important motivator in understanding the boundary between explosion and collapse.

Difficulties associated with modeling convective regions in these degenerate interiors prevent us from evolving our **MESA** models all the way to oxygen ignition. On one hand, the presence of carbon provides an additional energy source that, once ignited at the lower densities associated with the  $^{24}\text{Mg}$  electron captures, can help heat the WD to oxygen ignition conditions. On the other hand, this energy release also seems likely to push the model towards convective instability and the development of a convective core can defer oxygen ignition to higher densities. Firm conclusions await improved modeling techniques.

Nonetheless, this work indicates that the inclusion of carbon burning alters the evolution from that previously described in the literature. Intriguingly, the range of carbon abundances seen in our WD models produce evolutionary variations of a magnitude such that one might expect them to lead to a diversity of outcomes. Including the effects of residual  $^{12}\text{C}$  in ONe WDs, and more generally moving towards increasingly realistic progenitor modeling, is an important ingredient in modeling of AIC going forward.

We thank Jared Brooks, Lars Bildsten, and Eliot Quataert for their involvement in early explorations in this vein. We thank them, Ken Shen, Rob Farmer, and Frank Timmes for helpful discussions. We thank the referee for useful comments. We thank Enrico Ramirez-Ruiz for his co-supervision of KR. KR also thanks the Koret Scholars program and the Lamat REU program for financial support. Support for this work was provided by NASA through Hubble Fellowship grant # HST-HF2-51382.001-A awarded by the Space Telescope Science Institute, which is operated by the Association of Universities for Research in Astronomy, Inc., for NASA, under contract NAS5-26555. This research made extensive use of NASA’s Astrophysics Data System.



*Software:* MESA (Paxton et al. 2011, 2013, 2015, 2018), Python (available from [python.org](http://python.org)), matplotlib (Hunter

2007), NumPy (van der Walt et al. 2011), `py_mesa_reader` (Wolf & Schwab 2017)

## REFERENCES

- Alastuey, A., & Jancovici, B. 1978, *ApJ*, 226, 1034, doi: [10.1086/156681](https://doi.org/10.1086/156681)
- Althaus, L. G., García-Berro, E., Isern, J., Córscico, A. H., & Rohrmann, R. D. 2007, *A&A*, 465, 249, doi: [10.1051/0004-6361:20066059](https://doi.org/10.1051/0004-6361:20066059)
- Bloecker, T. 1995, *A&A*, 297, 727
- Boyles, J., Lorimer, D. R., Turk, P. J., et al. 2011, *ApJ*, 742, 51, doi: [10.1088/0004-637X/742/1/51](https://doi.org/10.1088/0004-637X/742/1/51)
- Brooks, J., Bildsten, L., Schwab, J., & Paxton, B. 2016, *ApJ*, 821, 28, doi: [10.3847/0004-637X/821/1/28](https://doi.org/10.3847/0004-637X/821/1/28)
- Brooks, J., Schwab, J., Bildsten, L., Quataert, E., & Paxton, B. 2017, *ApJ*, 834, L9, doi: [10.3847/2041-8213/834/2/L9](https://doi.org/10.3847/2041-8213/834/2/L9)
- Camisassa, M. E., Althaus, L. G., Córscico, A. H., et al. 2018, ArXiv e-prints. <https://arxiv.org/abs/1807.03894>
- Canal, R., Isern, J., & Labay, J. 1992, *ApJL*, 398, L49, doi: [10.1086/186574](https://doi.org/10.1086/186574)
- Caughlan, G. R., & Fowler, W. A. 1988, *Atomic Data and Nuclear Data Tables*, 40, 283, doi: [10.1016/0092-640X\(88\)90009-5](https://doi.org/10.1016/0092-640X(88)90009-5)
- Chamulak, D. A., Brown, E. F., Timmes, F. X., & Dupczak, K. 2008, *ApJ*, 677, 160, doi: [10.1086/528944](https://doi.org/10.1086/528944)
- Denissenkov, P. A., Herwig, F., Truran, J. W., & Paxton, B. 2013, *ApJ*, 772, 37, doi: [10.1088/0004-637X/772/1/37](https://doi.org/10.1088/0004-637X/772/1/37)
- Doherty, C. L., Gil-Pons, P., Siess, L., & Lattanzio, J. C. 2017, *Publications of the Astronomical Society of Australia*, 34, e056, doi: [10.1017/pasa.2017.52](https://doi.org/10.1017/pasa.2017.52)
- Dominguez, I., Tornambe, A., & Isern, J. 1993, *ApJ*, 419, 268, doi: [10.1086/173480](https://doi.org/10.1086/173480)
- Farmer, R., Fields, C. E., & Timmes, F. X. 2015, *ApJ*, 807, 184, doi: [10.1088/0004-637X/807/2/184](https://doi.org/10.1088/0004-637X/807/2/184)
- Förster, F., Lesaffre, P., & Podsiadlowski, P. 2010, *ApJS*, 190, 334, doi: [10.1088/0067-0049/190/2/334](https://doi.org/10.1088/0067-0049/190/2/334)
- Fuller, G. M., Fowler, W. A., & Newman, M. J. 1985, *ApJ*, 293, 1, doi: [10.1086/163208](https://doi.org/10.1086/163208)
- Gänsicke, B. T., Koester, D., Girven, J., Marsh, T. R., & Steeghs, D. 2010, *Science*, 327, 188, doi: [10.1126/science.1180228](https://doi.org/10.1126/science.1180228)
- García-Berro, E., & Iben, I. 1994, *ApJ*, 434, 306, doi: [10.1086/174729](https://doi.org/10.1086/174729)
- Gasques, L. R., Afanasjev, A. V., Aguilera, E. F., et al. 2005, *PhRvC*, 72, 025806, doi: [10.1103/PhysRevC.72.025806](https://doi.org/10.1103/PhysRevC.72.025806)
- Gil-Pons, P., & Doherty, C. L. 2010, *Memorie della Societa Astronomica Italiana*, 81, 974
- Gil-Pons, P., & García-Berro, E. 2001, *A&A*, 375, 87, doi: [10.1051/0004-6361:20010828](https://doi.org/10.1051/0004-6361:20010828)
- . 2002, *A&A*, 396, 589, doi: [10.1051/0004-6361:20021416](https://doi.org/10.1051/0004-6361:20021416)
- Graboske, H. C., Dewitt, H. E., Grossman, A. S., & Cooper, M. S. 1973, *ApJ*, 181, 457, doi: [10.1086/152062](https://doi.org/10.1086/152062)
- Gutiérrez, J., Canal, R., & García-Berro, E. 2005, *A&A*, 435, 231, doi: [10.1051/0004-6361:20042254](https://doi.org/10.1051/0004-6361:20042254)
- Gutierrez, J., Garcia-Berro, E., Iben, Jr., I., et al. 1996, *ApJ*, 459, 701, doi: [10.1086/176934](https://doi.org/10.1086/176934)
- Hashimoto, M., Iwamoto, K., & Nomoto, K. 1993, *ApJL*, 414, L105, doi: [10.1086/187007](https://doi.org/10.1086/187007)
- Heger, A., Langer, N., & Woosley, S. E. 2000, *ApJ*, 528, 368, doi: [10.1086/308158](https://doi.org/10.1086/308158)
- Heger, A., Woosley, S. E., & Spruit, H. C. 2005, *ApJ*, 626, 350, doi: [10.1086/429868](https://doi.org/10.1086/429868)
- Herwig, F. 2000, *A&A*, 360, 952
- Hunter, J. D. 2007, *Computing In Science & Engineering*, 9, 90
- Itoh, N., Hayashi, H., Nishikawa, A., & Kohyama, Y. 1996, *ApJS*, 102, 411, doi: [10.1086/192264](https://doi.org/10.1086/192264)
- Itoh, N., Totsuji, H., Ichimaru, S., & Dewitt, H. E. 1979, *ApJ*, 234, 1079, doi: [10.1086/157590](https://doi.org/10.1086/157590)
- Jones, S., Ritter, C., Herwig, F., et al. 2016a, *MNRAS*, 455, 3848, doi: [10.1093/mnras/stv2488](https://doi.org/10.1093/mnras/stv2488)
- Jones, S., Röpkke, F. K., Pakmor, R., et al. 2016b, *A&A*, 593, A72, doi: [10.1051/0004-6361/201628321](https://doi.org/10.1051/0004-6361/201628321)
- Jones, S., Hirschi, R., Nomoto, K., et al. 2013, *ApJ*, 772, 150, doi: [10.1088/0004-637X/772/2/150](https://doi.org/10.1088/0004-637X/772/2/150)
- Kepler, S. O., Koester, D., & Ourique, G. 2016, *Science*, 352, 67, doi: [10.1126/science.aad6705](https://doi.org/10.1126/science.aad6705)
- Kippenhahn, R., Ruschenplatt, G., & Thomas, H.-C. 1980, *A&A*, 91, 175
- Langer, N., El Eid, M. F., & Fricke, K. J. 1985, *A&A*, 145, 179
- Lecoanet, D., Schwab, J., Quataert, E., et al. 2016, *ApJ*, 832, 71, doi: [10.3847/0004-637X/832/1/71](https://doi.org/10.3847/0004-637X/832/1/71)
- Lesaffre, P., Han, Z., Tout, C. A., Podsiadlowski, P., & Martin, R. G. 2006, *MNRAS*, 368, 187, doi: [10.1111/j.1365-2966.2006.10068.x](https://doi.org/10.1111/j.1365-2966.2006.10068.x)
- Lesaffre, P., Podsiadlowski, P., & Tout, C. A. 2005, *Nuclear Physics A*, 758, 463, doi: [10.1016/j.nuclphysa.2005.05.086](https://doi.org/10.1016/j.nuclphysa.2005.05.086)
- Leung, S.-C., & Nomoto, K. 2017, *Mem. Soc. Astron. Italiana*, 88, 266
- Lyne, A. G., Manchester, R. N., & D’Amico, N. 1996, *ApJL*, 460, L41, doi: [10.1086/309972](https://doi.org/10.1086/309972)



- Maoz, D., Mannucci, F., & Nelemans, G. 2014, *ARA&A*, 52, 107, doi: [10.1146/annurev-astro-082812-141031](https://doi.org/10.1146/annurev-astro-082812-141031)
- Martínez-Pinedo, G., Lam, Y. H., Langanke, K., Zegers, R. G. T., & Sullivan, C. 2014, *PhRvC*, 89, 045806, doi: [10.1103/PhysRevC.89.045806](https://doi.org/10.1103/PhysRevC.89.045806)
- Meynet, G., & Maeder, A. 1997, *A&A*, 321, 465
- Miyaji, S., & Nomoto, K. 1987, *ApJ*, 318, 307, doi: [10.1086/165368](https://doi.org/10.1086/165368)
- Miyaji, S., Nomoto, K., Yokoi, K., & Sugimoto, D. 1980, *PASJ*, 32, 303
- Nomoto, K. 1984, *ApJ*, 277, 791, doi: [10.1086/161749](https://doi.org/10.1086/161749)
- . 1987, *ApJ*, 322, 206, doi: [10.1086/165716](https://doi.org/10.1086/165716)
- Nomoto, K., & Kondo, Y. 1991, *ApJL*, 367, L19, doi: [10.1086/185922](https://doi.org/10.1086/185922)
- Nomoto, K., Miyaji, S., Sugimoto, D., & Yokoi, K. 1979, in *IAU Colloq. 53: White Dwarfs and Variable Degenerate Stars*, ed. H. M. van Horn & V. Weidemann, 56–60
- Paczynski, B. 1971, *AcA*, 21, 271
- . 1973, *Astrophys. Lett.*, 15, 147
- Paxton, B., Bildsten, L., Dotter, A., et al. 2011, *ApJS*, 192, 3, doi: [10.1088/0067-0049/192/1/3](https://doi.org/10.1088/0067-0049/192/1/3)
- Paxton, B., Cantiello, M., Arras, P., et al. 2013, *ApJS*, 208, 4, doi: [10.1088/0067-0049/208/1/4](https://doi.org/10.1088/0067-0049/208/1/4)
- Paxton, B., Marchant, P., Schwab, J., et al. 2015, *ApJS*, 220, 15, doi: [10.1088/0067-0049/220/1/15](https://doi.org/10.1088/0067-0049/220/1/15)
- Paxton, B., Schwab, J., Bauer, E. B., et al. 2018, *ApJS*, 234, 34, doi: [10.3847/1538-4365/aaa5a8](https://doi.org/10.3847/1538-4365/aaa5a8)
- Piro, A. L., & Bildsten, L. 2008, *ApJ*, 673, 1009, doi: [10.1086/524189](https://doi.org/10.1086/524189)
- Piro, A. L., & Chang, P. 2008, *ApJ*, 678, 1158, doi: [10.1086/529368](https://doi.org/10.1086/529368)
- Potekhin, A. Y., & Chabrier, G. 2000, *PhRvE*, 62, 8554, doi: [10.1103/PhysRevE.62.8554](https://doi.org/10.1103/PhysRevE.62.8554)
- Raddi, R., Hollands, M. A., Koester, D., et al. 2018, *ApJ*, 858, 3, doi: [10.3847/1538-4357/aab899](https://doi.org/10.3847/1538-4357/aab899)
- Reimers, D. 1975, *Memoires of the Societe Royale des Sciences de Liege*, 8, 369
- Ritossa, C., Garcia-Berro, E., & Iben, Jr., I. 1996, *ApJ*, 460, 489, doi: [10.1086/176987](https://doi.org/10.1086/176987)
- Ritossa, C., García-Berro, E., & Iben, Jr., I. 1999, *ApJ*, 515, 381, doi: [10.1086/307017](https://doi.org/10.1086/307017)
- Ruiter, A. J., Ferrario, L., Belczynski, K., et al. 2018, *ArXiv e-prints*. <https://arxiv.org/abs/1802.02437>
- Schwab, J., Bildsten, L., & Quataert, E. 2017a, *MNRAS*, 472, 3390, doi: [10.1093/mnras/stx2169](https://doi.org/10.1093/mnras/stx2169)
- Schwab, J., Martínez-Rodríguez, H., Piro, A. L., & Badenes, C. 2017b, *ApJ*, 851, 105, doi: [10.3847/1538-4357/aa9a3c](https://doi.org/10.3847/1538-4357/aa9a3c)
- Schwab, J., Quataert, E., & Bildsten, L. 2015, *MNRAS*, 453, 1910, doi: [10.1093/mnras/stv1804](https://doi.org/10.1093/mnras/stv1804)
- Segretain, L., & Chabrier, G. 1993, *A&A*, 271, L13
- Siess, L. 2006, *A&A*, 448, 717, doi: [10.1051/0004-6361:20053043](https://doi.org/10.1051/0004-6361:20053043)
- . 2007, *A&A*, 476, 893, doi: [10.1051/0004-6361:20078132](https://doi.org/10.1051/0004-6361:20078132)
- . 2009, *A&A*, 497, 463, doi: [10.1051/0004-6361/200811362](https://doi.org/10.1051/0004-6361/200811362)
- Suzuki, T., Toki, H., & Nomoto, K. 2016, *ApJ*, 817, 163, doi: [10.3847/0004-637X/817/2/163](https://doi.org/10.3847/0004-637X/817/2/163)
- Takahashi, K., Yoshida, T., & Umeda, H. 2013, *ApJ*, 771, 28, doi: [10.1088/0004-637X/771/1/28](https://doi.org/10.1088/0004-637X/771/1/28)
- Tauris, T. M., Langer, N., & Podsiadlowski, P. 2015, *MNRAS*, 451, 2123, doi: [10.1093/mnras/stv990](https://doi.org/10.1093/mnras/stv990)
- Timmes, F. X., & Woosley, S. E. 1992, *ApJ*, 396, 649, doi: [10.1086/171746](https://doi.org/10.1086/171746)
- Timmes, F. X., Woosley, S. E., & Taam, R. E. 1994, *ApJ*, 420, 348, doi: [10.1086/173565](https://doi.org/10.1086/173565)
- Toki, H., Suzuki, T., Nomoto, K., Jones, S., & Hirschi, R. 2013, *PhRvC*, 88, 015806, doi: [10.1103/PhysRevC.88.015806](https://doi.org/10.1103/PhysRevC.88.015806)
- van der Walt, S., Colbert, S. C., & Varoquaux, G. 2011, *Computing in Science Engineering*, 13, 22, doi: [10.1109/MCSE.2011.37](https://doi.org/10.1109/MCSE.2011.37)
- Vennes, S., Nemeth, P., Kawka, A., et al. 2017, *Science*, 357, 680, doi: [10.1126/science.aam8378](https://doi.org/10.1126/science.aam8378)
- Wolf, B., & Schwab, J. 2017, *wmwolf/py\_mesa\_reader: Interact with MESA Output*, doi: [10.5281/zenodo.826958](https://doi.org/10.5281/zenodo.826958), <https://doi.org/10.5281/zenodo.826958>
- Wolf, W. M., Bildsten, L., Brooks, J., & Paxton, B. 2013, *ApJ*, 777, 136, doi: [10.1088/0004-637X/777/2/136](https://doi.org/10.1088/0004-637X/777/2/136)
- Yakovlev, D. G., Gasques, L. R., Afanasjev, A. V., Beard, M., & Wiescher, M. 2006, *PhRvC*, 74, 035803, doi: [10.1103/PhysRevC.74.035803](https://doi.org/10.1103/PhysRevC.74.035803)